In operando adjustable orbital polarization in $LaNiO_3$ thin films

Hari Babu Vasili,[1,*] David Pesquera,[2] Manuel Valvidares,[1] Pierluigi Gargiani,[1] Eric Pellegrin,[1] Federica Bondino,[3] Elena Magnano,[3] Alessandro Barla,[4] and Josep Fontcuberta[2,†]

[1]*ALBA Synchrotron Light Source, E-08290 Cerdanyola del Vallès, Barcelona, Catalonia, Spain*
[2]*Institut de Ciència de Materials de Barcelona (ICMAB-CSIC), Campus UAB, 08193, Bellaterra, Catalonia, Spain*
[3]*Istituto Officina dei Materiali (IOM), Consiglio Nazionale delle Ricerche (CNR), I-34149 Trieste, Italy*
[4]*Istituto di Struttura della Materia (ISM), Consiglio Nazionale delle Ricerche (CNR), I-34149 Trieste, Italy*

(Received 20 May 2019; revised manuscript received 29 January 2020; accepted 26 February 2020; published 7 April 2020)

The different occupancy of electronic orbitals, the so-called *orbital polarization*, is a key parameter determining electric and magnetic properties of materials. Here we report on the demonstration of *in operando* voltage-controlled tuning of the orbital occupation in $LaNiO_3$ epitaxial thin films grown on piezoelectric substrates. The different static contributions to the orbital occupation are disentangled, namely the epitaxial strain and the surface symmetry breaking, and the superimposed electric-field controlled orbital polarization are determined by x-ray linear dichroism at the Ni $L_{2,3}$ edges. The voltage-controlled orbital polarization allows changing the orbital polarization by about an additional 50%.

DOI: 10.1103/PhysRevMaterials.4.044404

I. INTRODUCTION

Manipulating the $3d$ orbital states in transition-metal oxides opens a way to create artificial materials by design. One can envision, for instance, the possibility of engineering materials which emulate the electronic and orbital configuration of high-temperature superconductors (HTSc) [1–3]. Nickelate perovskite $RNiO_3$ (R is a trivalent rare-earth ion), and in particular $LaNiO_3$ (LNO) (the only compound in the series showing metallic behavior at all temperatures) [4], are promising candidates for this purpose. The electronic structure of Ni^{3+} is composed of a full t_{2g} band and a single-electron occupancy in the e_g states ($3d^7 : {t_{2g}}^6 {e_g}^1$) which—due to the essentially isotropic three-dimensional character of the Ni–O bonding network in bulk compounds—are degenerate. On the other hand, cuprate HTSc show a $Cu^{2+} : 3d^9$ configuration where, due to the two-dimensional layered structure, the e_g states are 100% orbitally polarized, i.e., the single hole is located in an $x^2 - y^2$ state of the crystal-field-split e_g:(z^2, $x^2 - y^2$)-manifold. Achieving such an analogous configuration in LNO would require lifting the $Ni^{3+}3d$-e_g orbital degeneracy. This could eventually result in a preferential electron occupancy of one of the e_g orbitals, thus giving rise to a large "orbital polarization" (henceforth, abbreviated as "OP") of the d states forming the conduction band.

Different ways have been explored to modulate the OP in nickelates: (*i*) strain engineering [5,6] (*ii*) electron confinement by sandwiching LNO layers between insulating layers [6], and (*iii*) charge transfer in trilayer heterostructures, mimicking to some extent the role of free surfaces, or inversion symmetry breaking [7], as recently reviewed by Disa *et al.* [8].

The strain-induced modulation of orbital occupancy has been proven to be effective in manganite thin films [9,10] as well as in the nickelates [5,6], leading to a preferential $x^2 - y^2$ ($3z^2 - r^2$) occupancy for tensile (compressive) strain. Substrate-induced epitaxial strain can be accommodated by tetragonal distortion of the coordination polyhedra of the metal ions as well as by octahedral rotations; their relative role can be different for the compressive or tensile strain [11] and it could thus lead to asymmetric effects of strain on OP. Indeed, early results suggested an intriguing asymmetric response of OP to tensile/compressive elastic strain in LNO films [4]; however, it was later argued that this difference in orbital polarization could be related to the contribution of surface states rather than elastic strain, which originates from symmetry breaking at the free surface [5], as already reported in manganite films [10] and other similar systems [12,13].

In bilayer structures, such as $LaNiO_3/LaAlO_3$ superlattices [6]—where ultrathin LNO films are confined between the $LaAlO_3$ insulating layer—the charge hopping along the z direction (i.e., perpendicular to the NiO_2 planes) is canceled, thus producing a narrowing of the electronic bandwidth associated with the z^2 orbitals. Therefore, subsequent filling of the $3d$ orbitals should shift the Fermi level towards the $x^2 - y^2$ band, thus increasing the OP. Experimental results on $LaNiO_3/LaTiO_3$ superlattices have confirmed this view [7]. This charge transfer also promotes the appearance of an electric field that expands the Ni–O–Ti bonds along the z axis which pushes further down the z^2 orbital, causing an enhanced OP. It was predicted that OP could be ultimately raised by including the symmetry breaking of the Ni coordination polyhedra in the tricolor superlattice $LaNiO_3/LaTiO_3/LaAlO_3$. Combining the strain and confinement could lead to a change of OP by about 25% [6], whereas the symmetry-breaking superlattices promised OP of 55%, which is in good agreement with experiments [7].

*hbvasili@gmail.com
†fontcuberta@icmab.cat

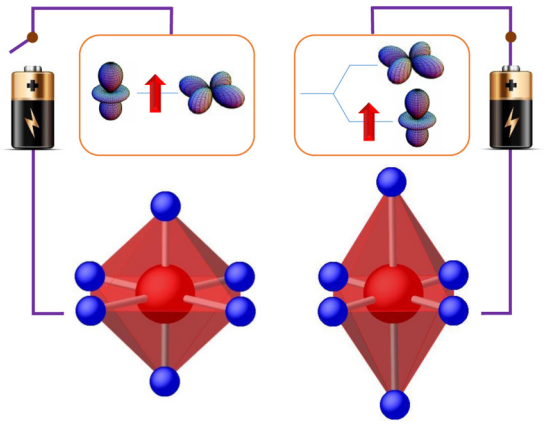

FIG. 1. Straining the NiO_6 octahedron by applied electric field causes degeneracy breaking at $3d$ e_g orbitals. The ON (closed) and OFF (open) switch state of the battery refers to strained and unstrained states of the octahedron, respectively.

All in all, in the LNO heterostructures summarized above, the orbital occupancy is determined by a combination of the electronic properties of the materials sandwiching the LNO film, the internal polar fields acting on the LNO layer, and/or the epitaxial strain imposed by the substrates. Therefore, the design of LNO heterostructures determines OP and ultimately fixes the electronic properties of the LNO films.

Aiming at the development of reconfigurable devices, it would be highly desirable to design oxide-based systems where OP can be tuned *in situ* by using an appropriate stimulus. To this goal, here we report orbital polarization in LNO films grown on piezoelectric substrates [e.g., $Pb(Mg_{1/3}Nb_{2/3})O_3$–$PbTiO_3$ (PMN-PT)]. Piezoelectric substrates, on the basis of converse piezoelectric effect, allow a voltage-controlled deformation of the material. If an active layer is suitably grown and epitaxially clamped to a piezoelectric substrate, a voltage-controlled strain can be transmitted to the functional film and so its properties can be tailored *ad hoc*, as illustrated in Fig. 1, for, e.g., breaking the degeneracy of e_g orbitals. This approach has been extensively used, for example, to modulate the magnetic properties of metals and oxides, namely the magnetization and magnetic anisotropy [14–16] as well as to tune the metal-insulator transitions in manganites [17] and vanadates [18]. This approach has been recently used to attempt the tuning of the temperature (T_{MI}) of the metal-insulator (M-I) transition of $NdNiO_3$ thin films [19].

Besides this piezostrain action/response, it worth noticing that piezoelectric substrates under applied voltage may also influence an upper-lying film via the presence of polarization charges. Therefore, piezosubstrates could allow, in principle, the emulation of the electric field existing in tricolor superlattices and take advantage of the polarization-related interfacial bonding [20], with the additional benefit that these effects become controllable *in situ* by an external voltage.

In this paper, we explore the orbital polarization of epitaxial LNO thin films, with the ultimate goal of achieving a large and *in situ* tunable orbital polarization. We exploit the well-known sensitivity of linearly polarized x-ray absorption spectroscopy (XAS) at transition-metal $L_{2,3}$ absorption edges and the x-ray linear dichroism (XLD) as a probing tool for determining the OP. Earlier experiments on manganite films grown on ferroelectric/piezoelectric substrates have demonstrated that using XLD, one can determine voltage-induced changes of orbital polarization of $3d$ states. For instance, Preziosi *et al.* [21] have reported the XLD data at the Mn $L_{2,3}$ edges of $La_{0.825}Sr_{0.175}MnO_3$ films grown on ferroelectric $PbZr_{0.52}Ti_{0.48}O_3$ (PZT) and observed a change of orbital occupation depending upon the polarization state of the ferroelectric layer. It was argued that this observation was due to the changes of Mn–O–Mn bonds at the interface which are distinct for up/down polar states of the ferroelectric substrate. Heidler *et al.* [22] reported the XLD on $La_{0.7}Sr_{0.3}MnO_3$ films grown on PMN-PT(011) and observed a change of orbital occupation under the electric-field biasing, which was attributed to the elastic response of the magnetic layer to the piezodeformation of the substrate. Interestingly, similar experiments performed on Co/PMN-PT(011) suggested that the most relevant effects are related to polarization-induced charge reconstruction, rather than to strain, at the electrode (Co) [23]. These few examples illustrate the complexity of the problem.

Our paper is organized as follows. To establish a self-contained starting point, we first monitor the impact of epitaxial strain on OP, by determining the OP in LNO films grown on various substrates imposing different epitaxial strain. Next, in order to disentangle the unavoidable contribution of symmetry breaking at the free surface of the films on OP, we report measurements on LNO films of different thicknesses but having a constant strain state. Armed with this knowledge, we proceed next to determine OP in LNO films grown on piezosubstrates (PMN-PT) and its dependence on the electric field biasing the substrate, by measuring the XLD at the Ni $L_{2,3}$ edges at *in operando* conditions. Our data show a dramatic control of OP by the voltage, as sketched in Fig. 1, which illustrates the piezodeformation of the substrate. Interestingly, the voltage-induced changes of the orbital occupancy are found to be much larger (about a fivefold increase) than those expected on the basis of an elastic deformation induced by a potential clamping of the LNO film to the underlying piezoelectric PMN-PT substrate. Several scenarios are analyzed to address this giant sensitivity of LNO orbital polarization to the voltage-induced substrate piezoresponse; we argue that this enhanced response may be a signature of either the known distinctive piezoelectric properties of PMN-PT surfaces or result from a genuinely different response of the LNO lattice to epitaxial strain induced during high-temperature film growth and possible room-temperature dynamic substrate-induced deformations. In any event, it will be shown that although polarization can be voltage tuned by about $\Delta P/P = 66\%$ (where P is defined as $3d$ orbital polarization), the most critical observations are that the absolute values of P remain within an 8 to 3% range and that the voltage-controlled term favors a $3z^2 - r^2$ occupation that competes with the PMN-PT epitaxial mismatch favoring the $x^2 - y^2$ occupancy, thus challenging achieving the much-desired full $x^2 - y^2$ occupation. To this respect, we propose some strategies that may allow reverting the competition among epitaxial strain and piezocontrolled orbital polarization contributions.

TABLE I. Lattice parameters (a, c), mismatch (in %), and in-plane strain (ε) (in %) values for LNO films grown on various substrates. Positive and negative signs correspond to in-plane tensile and compressive lattice mismatch and strain, respectively.

Substrate	Mismatch[a] (%)	a(Å)	c(Å)	Strain (ε)[b] (%)
STO	+1.96	3.89	3.80	+1.57
LSAT	+0.99	3.86	3.82	+0.78
LAO	−1.12	3.80	3.91	−0.78
PMN-PT	+5.17	3.87[c]	3.78	+1.0[c]
			$a_{\mathrm{LNO}} = 3.83$ Å	

[a]Mismatch $=(a_{\mathrm{sub}} - a_{\mathrm{LNO}})/a_{\mathrm{LNO}}$.
[b]Strain $=(a_{\mathrm{film}} - a_{\mathrm{LNO}})/a_{\mathrm{LNO}}$.
[c]Determined from reciprocal space maps of LNO(10 nm)/STO(5 nm)//PMN-PT.

II. EXPERIMENTAL DETAILS

We grew epitaxial LNO films on various single-crystalline substrates by pulsed laser deposition at an oxygen pressure of 0.15 mbar and a substrate temperature of 700 °C. The number of laser pulses was varied to obtain films with nominal thickness t between 2 and 14 nm, according to the growth rate calibration. For every given number of laser pulses, films on different substrates were grown simultaneously to minimize spurious thickness variations. We used single-crystalline substrates with (001) orientation having a (pseudo)cubic lattice parameter either smaller [in case of $LaAlO_3$ (LAO)] or larger [for $(LaAlO_3)_{0.3}$-$(Sr_2AlTaO_6)_{0.7}$ (LSAT) and $SrTiO_3$ (STO)] than the pseudocubic parameter of LNO (mismatch values are given in Table I). Similarly, 10-nm-thick LNO films were grown on bare PMN-PT(001) substrates and also on STO-buffered (5 nm) PMN-PT(001) substrates.

The structural characteristics of the LNO films were investigated by x-ray diffraction (XRD) using the θ-2θ patterns for determining the out-of-plane cell parameters and grazing-incidence scans for the in-plane cell parameters via in-plane (220) reflections and reciprocal space maps. Further growth and structural characterization details can be found in Ref. [24]. The biaxial tensile strain promoted by the cubic (or nearly cubic) substrates induces a contraction of the c-axis lattice parameter for films grown on STO and LSAT, while the films on LAO show an out-of-plane lattice parameter larger than bulk LNO, as expected from compressive strain-induced tetragonal distortions of the films. The out-of-plane lattice parameters (c) of the films were determined by doing XRD simulations taking into account the interference effects between the diffracted waves from films and substrates [25]. The best-fitting curves lead to the c values given in Table I. The in-plane cell parameters (a) extracted from grazing-incidence XRD experiments are also included in Table I. For completeness we also include in Table I the XRD data of the LNO films on PMN-PT to be discussed latter, as well as the calculated structural mismatch and the in-plane strain measured on all films. Within our diffractometer resolution, and in good agreement with previous reports [24], we have found in the reciprocal space maps no evidence of extra peaks which may indicate a lower than tetragonal symmetry (i.e., monoclinic). Details on structural characterization are in Ref. [26].

All LNO films reported here display a metallic behavior, with room-temperature resistivities $<0.9\,\mathrm{m\Omega\,cm}$ and $<3\,\mathrm{m\Omega\,cm}$ for thicknesses of 14 and 2 nm, respectively [26].

We measured the XAS of the samples at the Ni-$L_{2,3}$ edges at 300 K using linearly (either horizontal or vertical) polarized light and probed the XLD as the difference between the two light polarizations. To get access to the subtle differences in the orbital occupancy of e_g-($x^2 - y^2$ and $3z^2 - r^2$) states, the x-ray absorption has to be taken for $\boldsymbol{E}//$ab and for $\boldsymbol{E}//c$ (later shortened as E_{ab} and E_c, respectively, where ab and c indicate in-plane and out-of-plane x-ray electric-field $\boldsymbol{E}$ directions, respectively). Due to geometrical constraints, following common practice, we collected the spectra in grazing incidence with the x-ray incidence direction $\boldsymbol{k}$ at $\theta = 60^\circ$ with respect to the surface normal. Thus, the light polarization vector $\boldsymbol{E}$ is parallel (vertical polarization) or nearly perpendicular (horizontal polarization) to the film surface normal. The geometric effect due to the non-fully-grazing incidence ($\theta = 60^\circ$) is corrected in the determination of P as described in Refs. [27,28]. The photocurrent was measured in the total electron yield (TEY) mode. XAS data in TEY mode can be robustly collected at 300 K and at low temperature [26], confirming the metallic nature of the LNO films. Average XAS spectra were obtained by averaging the intensities of both linear polarizations—parallel to the surface normal, $I(E_c)$, and perpendicular to it, $I(E_{ab})$– as $I_0 = [I(E_c) + I(E_{ab})]/2$. The XLD signal was obtained as $I(E_{ab})$–$I(E_c)$. The XAS experiments were performed at two different synchrotrons: (*i*) "substrate-induced strain"— experiments at BACH [29], Elettra light source (Italy) and (*ii*) "electric-field-controlled strain" experiments at BL29 BOREAS [30], ALBA synchrotron (Spain), using a specially designed setup.

In lanthanum nickelates, the La M_4 absorption edge overlaps with the pre-edge side of the Ni L_3 edge [26]. We have removed this La M_4 contribution by subtracting the La-M_4 spectra measured on La-containing perovskite oxides, either $LaCoO_3$ (at BACH beamline) or $La_{2/3}Sr_{1/3}MnO_3$ (at BOREAS beamline), during the experiments. After subtracting these reference spectra, the Ni-L_3 peak splitting and the Ni-L_3 XLD remain unaffected. On the other hand, the Ni L_2 edge is not affected at all by the La overlapping.

In Fig. 2(a) we show, as an illustrative example, the Ni-$L_{2,3}$ XAS of an LNO film after subtracting the La-M_4 peak. It can be appreciated that the resulting Ni spectra are in close agreement with the reported spectra for Ni^{3+} oxides (see Refs. [31–34]). A detailed inspection of the Ni L_3 edge reveals a double-peak structure (Ref. [26]) whose energy splitting and relative intensities are related to the Ni-O hybridization strength [32–34] which will not be discussed

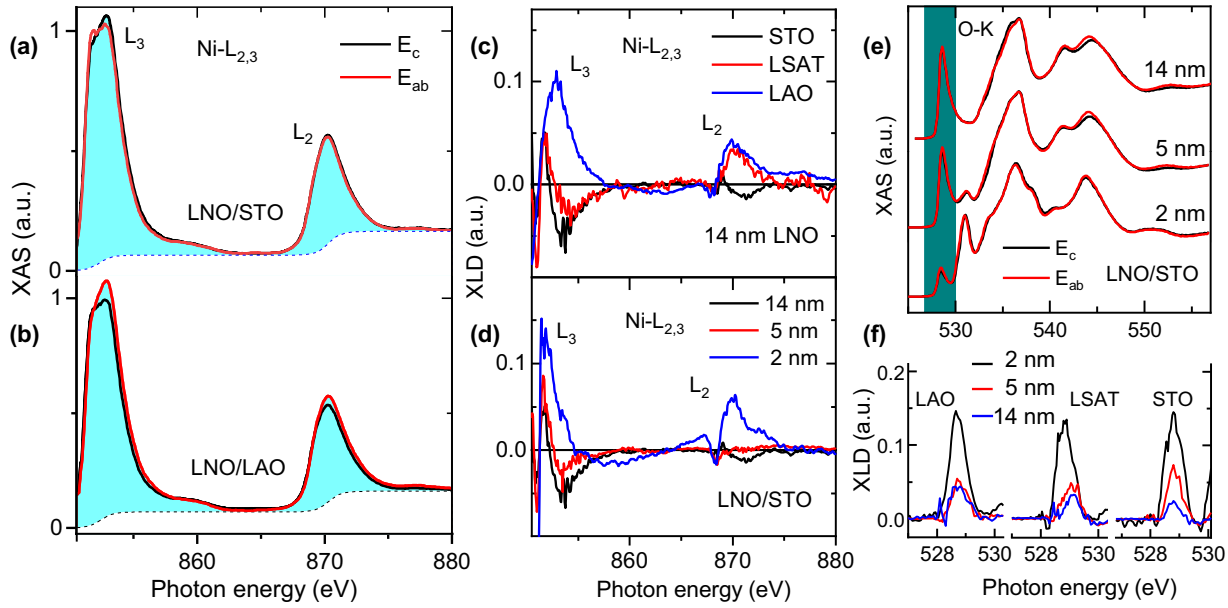

FIG. 2. (a), (b) Ni $L_{2,3}$ XAS (for $E||c$ and $E||ab$ polarizations) of 14-nm LNO thin films on STO and LAO, respectively. The spectra are plotted after subtracting the La M_4 and normalizing to their average L_3 peak intensity (E_0). (c) The Ni $L_{2,3}$ XLD (i.e., $E||ab - E||c$) of LNO(14 nm) films grown on different (001)-oriented single-crystalline substrates indicates that the STO and LAO (tensile and compressive strained) exhibit opposite signs corresponding to the $x^2 - y^2$ and $3z^2 - r^2$ orbital occupancy, respectively, while the LSAT remains intermediate. (d) The Ni $L_{2,3}$ XLD of 2, 5, and 14-nm LNO on STO indicate that the sign and magnitude of XLD changes, indicating a larger $3z^2 - r^2$ orbital occupancy when reducing thickness. (e) The O K-edge XAS for different thicknesses of LNO films on STO substrates. (f) Thickness variation of the O K XLD for the LNO films on LAO, LSAT, and STO substrates.

here. The Ni-XLD cannot be affected by the La-M_4 because the symmetric $4d^{10}5s^25p^6$ electronic configuration of La^{3+} produces a null XLD contribution. Therefore, the XLD provides reliable information on the $3d$ electron orbital occupancy within the $x^2 - y^2$ and $3z^2 - r^2$ states of the Ni^{3+} e_g– manifold ($d^7 : t_{2g}{}^6e_g{}^1$). The hole ratio (X) of unoccupied final e_g states (ratio of $3z^2 - r^2$ to $x^2 - y^2$) can be determined by using the integrated intensities I_c and I_{ab} of the Ni $L_{2,3}$ edges (excluding the La-overlapping vicinities, as shown in Figs. 2(a) and 2(b) and is given by [27]

$$X = \frac{h_{3z^2-r^2}}{h_{x^2-y^2}} = \frac{3I_c}{4I_{ab} - I_c} \tag{1}$$

where h_i is the hole concentration corresponding to the $3z^2 - r^2$ or $x^2 - y^2$ orbitals, and I_c and I_{ab} are the integrals of the XAS spectra $I(E_c)$ and $I(E_{ab})$ within the light cyan-colored region of Figs. 2(a) and 2(b) after removing the background by taking a step function. The $3d$ orbital polarization, P, is defined as

$$P = \frac{(n_{x^2-y^2}) - (n_{3z^2-r^2})}{(n_{x^2-y^2}) + (n_{3z^2-r^2})} = \left(\frac{4}{n_{e_g}} - 1\right)\left(\frac{X-1}{X+1}\right), \tag{2}$$

where n_i represents the electron occupancy at the corresponding $3z^2 - r^2$ and $x^2 - y^2$ orbitals. The "P" can be rewritten in terms of the experimental observable "X" as indicated; here, n_{e_g} represents the total number of electrons at the Ni e_g orbitals, that in the simplest ionic picture ($Ni^{3+} = 3d^7$) would correspond to $n_{e_g} = 1$. However, we stress that X, rather than P, is the experimental observable in XLD data [35].

III. RESULTS AND DISCUSSION

We start the discussion with the first part of the results, i.e., the substrate-induced elastic strain effects on the Ni $3d$ orbital polarization derived from the XLD data. To this purpose, we have used LNO films with 2, 5, and 14-nm thicknesses on various (001)-oriented single-crystalline substrates (causing either tensile or compressive strain). In Fig. 2(c) we show the Ni-$L_{2,3}$ XLD spectra of 14-nm-thick LNO films under different epitaxial strain. The XLD data are plotted after normalizing the spectral weight of the corresponding isotropic XAS to one at the L_3 peak, as shown in Figs. 2(a) and 2(b) for LNO films on STO and LAO, respectively. It can be readily appreciated from the above data that the LNO film grown on the LAO substrate (compressively strained) shows a positive XLD signal at both L_2 and L_3 edges. This indicates a larger x-ray absorption for the in-plane oriented orbitals (larger $h_{x^2-y^2}$) than for the out-of-plane ones ($h_{3z^2-r^2}$). In contrast, the LNO film on STO (tensile strained) displays a clearly negative XLD signal (i.e., more available states in the out-of-plane $3z^2 - r^2$ orbitals). The sample on LSAT (slight tensile strain) shows intermediate, barely positive, XLD signal. Overall, the XLD spectra immediately reflect the $3d$ orbital occupancy.

As aforementioned, by taking I_c and I_{ab} we have evaluated the hole occupancy ratio X, as given in Eq. (1), as a function of strain [see Fig. 3(a), black colored points and shaded line for the 14-nm-thick films]. The x-axis shows the in-plane strain (ε)– either positive (LSAT, STO) or negative (LAO)—acting on the LNO films. For convenience, we include in Fig. 3(a) (right axis) the orbital polarization, P, calculated by assuming $n_{e_g} = 1$. It can be observed that $X(\varepsilon)$ increases

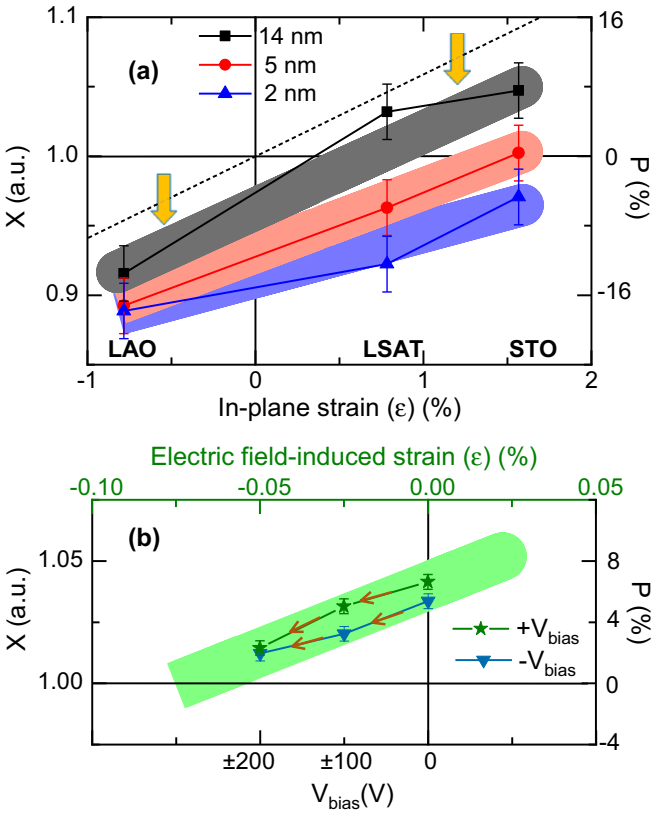

FIG. 3. (a) Hole ratio (X) (left axis) and electron orbital polarization (P) (right axis) as a function of substrate-induced epitaxial in-plane strain (ε) for the LNO films (2, 5, and 14 nm) on different strains (tensile for STO and LSAT, compressive for LAO). Dashed oblique line passing through the origin ($\varepsilon = 0, X = 1$) indicates the apparent orbital polarization if strain-only phenomena were considered. However, the yellow arrows emphasized the observed downward shift in X due to the symmetry breaking at surface-induced ($3z^2 - r^2$) orbital polarization. (b) The X and P values of LNO film in LNO(10 nm)/STO(5 nm)//PMN-PT heterostructure as a function of the voltage (V_{bias}) applied across the PMN-PT substrate (bottom axis). Top axis show the maximal possible in-plane (tensile) strain caused by the STO//PMN-PT at some selected $\pm V_{\text{bias}}$ values, assuming a fully elastic response of LNO to PMN-PT deformation.

with ε indicating that the $h_{3z^2-r^2}/h_{x^2-y^2}$ ratio increases with the tensile strain, reflecting a strain-induced stabilization (and thus higher electron occupancy) of the $x^2 - y^2$ states; reciprocally, X decreases when increasing the compressive strain, reflecting the strain-induced stabilization (and thus larger electron occupancy) of the $3z^2 - r^2$ orbitals. Interestingly, however, the overall trend appears to be shifted downwards [see the dashed line with yellow arrows in Fig. 3(a)]. Indeed, for a nominally strain-free film ($\varepsilon = 0$), Fig. 3(a) indicates that P would be different from zero (i.e., $X < 1$) thus indicating that the $3z^2 - r^2$ orbitals are stabilized even when the epitaxial strain is absent ($\varepsilon = 0$). As already noticed in manganite thin films [10], this effect originates from the absence of apical oxygen atoms in the surface layers. To assess this scenario in nickelates, we have grown LNO films down to 2-nm thickness on each substrate, expecting to enhance the surface contribution in the thinner films.

In Fig. 2(d), we compare the XLD data of 2, 5, and 14-nm-thick LNO films grown on STO substrates. It is clear that, when reducing the film thickness, the XLD signal (both at the L_2 and the L_3 edges) becomes gradually more positive. This is reflected by a corresponding X reduction, as shown by the thickness-dependent $X(\varepsilon)$ data of Fig. 3(a). In other words, electrons within the free surface are preferentially localized at $3z^2 - r^2$ orbitals, i.e., the $3z^2 - r^2$ orbitals are pushed down in energy due to the symmetry breaking at the LNO surface. Therefore, the above data can be interpreted as follows: In the thicker films—where the bulk contribution of the film dominates the dichroic signal(s)—mostly strain effects (the so-called strain-induced orbital polarization) determine the measured orbital occupancy. However, when reducing the sample thickness, the signal originated at surface layers becomes more relevant and the XLD is dominated by the surface symmetry-breaking effects. To summarize, the tensile strained films show a positive P in the bulk regime, as expected from the strain effects, but a negative polarization emerges at the surface [see Fig. 3(a)].

A similar thickness-dependent XLD analysis has been performed on all the LNO films (2, 5, and 14 nm) grown on other substrates (LSAT and LAO) (Ref. [26]). In Fig. 3(a) we have plotted all the measured X and calculated P values as a function of both strain and thickness. An inspection of all these data confirms that, irrespective of the substrate, there is a similar enhancement of the $3z^2 - r^2$ occupancy at the surface of all the LNO films. A final test of this hypothesis has been performed by measuring the XLD of an LNO film that has been *on-purpose* grown and *in situ* capped with a layer of LAO to avoid surface contamination. As expected, the $3z^2 - r^2$ contribution associated with the symmetry breaking at the surface is found to be reduced [26].

To convey a clear message, we have so far assumed a purely ionic picture for the Ni–O bond, that is: Ni^{3+}-$2p^6$ electronic configuration. However, it is known that the wave function for $3d$ Ni in a Ni–O octahedron can be written as $\Phi_g = \alpha|3d^7\rangle + \beta|3d^8\underline{L}\rangle$, where $|\underline{L}\rangle$ indicates a hole in the O-$2p$ band, $\alpha^2 + \beta^2 = 1$ [36]. Therefore, it should be expected that the XAS at the O K edges also reflects the impact of strain and surface effects on the hybridization strength (β). Similarly, the selective occupation at the Ni-e_g orbitals derived above should translate into a selective occupancy of the corresponding ($p_{x,y,z}$) hybridized states, which may give rise to an observable XLD at the O K edges. Both features have been identified here through the analysis of the XAS and XLD at the oxygen K edge, particularly on the prepeak edges, which are most sensitive to the Ni $3d$–O $2p$ hybridization. Figure 2(e) illustrates the evolution of the O K-edge prepeak of LNO/STO with LNO thickness and in Fig. 2(f) we depict the XLD determined at O K-edge prepeak as a function of substrate and thickness. Quantitative analysis of these signals is challenged by the contribution of the substrate, which becomes relevant when reducing the thickness of LNO [26].

One can observe in Fig. 3(a) that epitaxial strain allows modifying the orbital polarization by as much as $\Delta X \approx 13\%$ ($\Delta P \approx 20\%$), corresponding to $\Delta X/\Delta\varepsilon \approx 6\%/\%$ ($\Delta P/\Delta\varepsilon \approx 9\%/\%$). This variation is in good agreement with the results ($\Delta X/\Delta\varepsilon \approx 9.5\%/\%$) reported for $(\text{LNO}/\text{ABO}_3)_{4uc}$

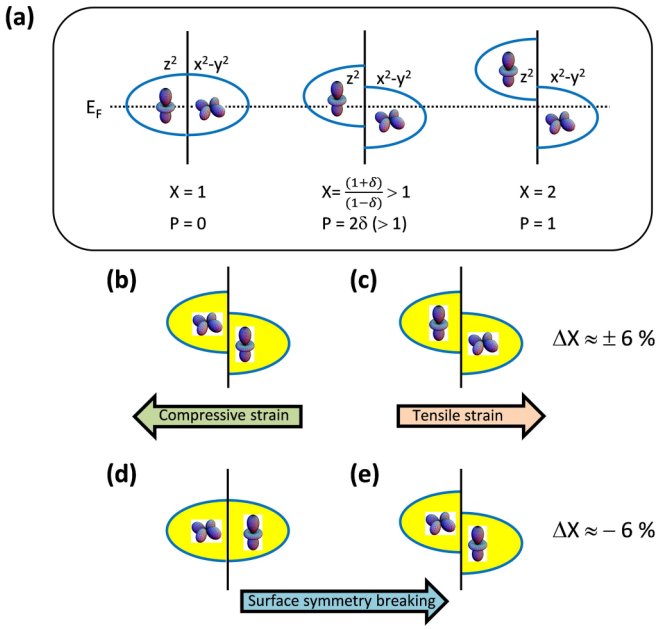

FIG. 4. (a) Sketches illustrating the orbital polarization definitions. (b), (c) Orbital polarization induced by compressive and tensile strain, respectively. (e) Surface-induced orbital polarization acting on a degenerate e_g orbital manifold (d).

superlattices [6]. From these observations, we assess that the strain stabilizes indistinctly both the $3z^2 - r^2$ and $x^2 - y^2$ states and thus the occupancy ratio ($h_{3z^2-r^2}/h_{x^2-y^2}$) can be regulated. However, one should notice that the measured values of the orbital polarization are rather modest. Indeed, full occupation of $x^2 - y^2$ orbitals corresponds to $X = 2$ ($P = 1$), as sketched in Fig. 4(a). The measured orbital polarization values roughly span from $X \approx +0.9$ to $1.05(-16\% < P < 8\%)$, as illustrated in Figs. 4(b) and 4(c).

Now, we discuss the second part of our work, concerning the effect of electric-field-induced elastic strain on the Ni $3d$ orbital polarization. Here, we have used LNO films with intermediate thickness (10 nm) on the piezosubstrate (PMN-PT) buffered with an STO layer (5 nm). While LNO films had been first grown directly on PMN-PT, their polycrystalline nature (Ref. [26]) precluded further use and we thus concentrate on the LNO films grown using the STO buffer layer. The XRD data reveal that the STO buffer film grown on PMN-PT exhibits, within the experimental resolution, the bulk STO cell parameters; therefore, as we have already described in the aforementioned substrate-induced elastic strain experiments, the LNO film is tensile strained (see data in Table I and the experimental results in Ref. [26]). In Fig. 5(a) we show a sketch illustrating the experimental arrangement for recording the XAS with an external bias voltage (V_{bias}) applied across the sample (LNO/STO//PMN-PT) perpendicular to the sample substrate. Briefly, a copper plate attached below the substrate was used as a bottom electrode. The metallic LNO film was connected, via a tee, to a grounded electrometer to record the TEY signal and to a DC power supply (battery box, up to ±200 V) to apply a V_{bias} across the PMN-PT, using LNO

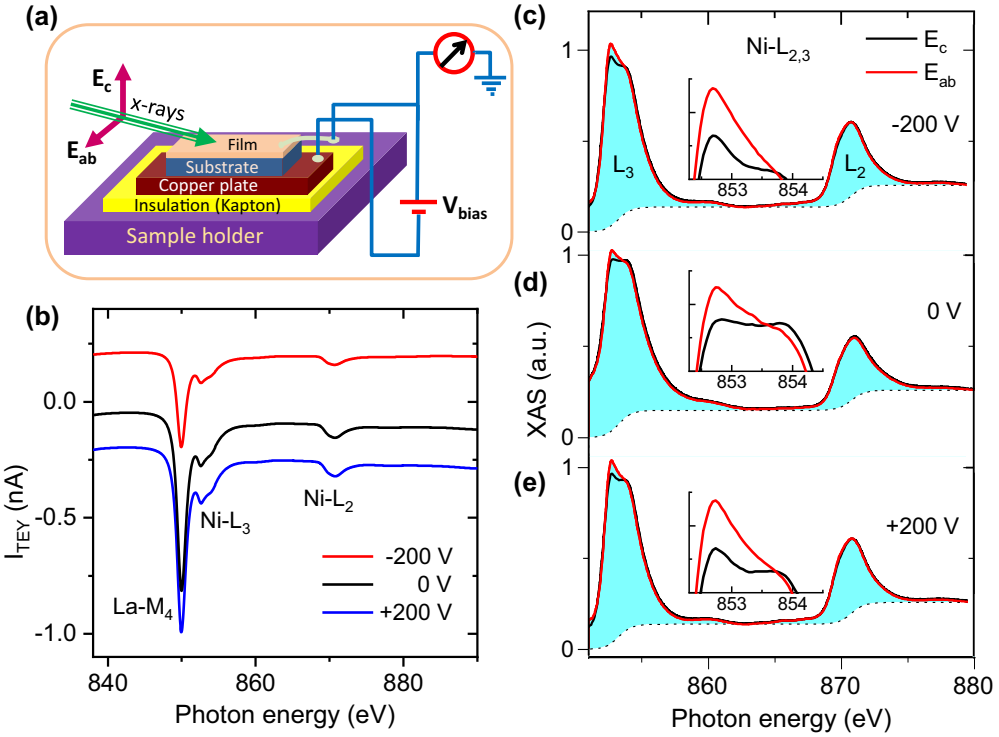

FIG. 5. (a) Sketch of the experimental arrangement to measure the XAS absorption in a voltage-biased LNO/STO//PMN-PT heterostructure. **(b)** The raw TEY signal at Ni $L_{2,3}$ edges collected with $V_{bias} = -200$ V, 0 V, and +200 V. (c)–(e) The Ni $L_{2,3}$ XAS recorded at $V_{bias} = -200$ V, 0 V, and + 200 V, respectively, using polarizations $\mathbf{E}_{ab}$ and $\mathbf{E}_c$ as indicated, after subtracting La-M_4. Insets in (c)–(e) are zooms of the L_3 peak data recorded with $\mathbf{E}_{ab}$ and $\mathbf{E}_c$, where dichroism is more evident. Integrated XAS values were taken from the light cyan-colored region after removing the step function.

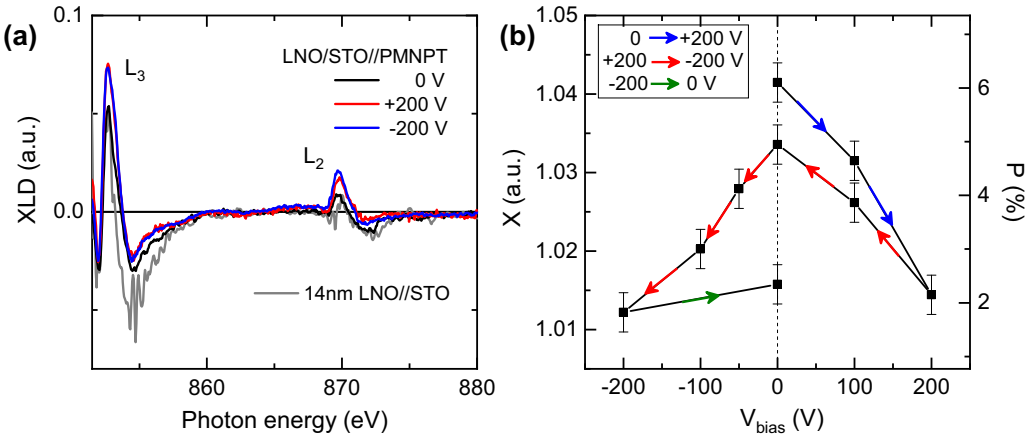

FIG. 6. (a) The Ni $L_{2,3}$ XLD of an LNO/STO//PMN-PT film at 0 V and ±200 V indicates that V_{bias} changes the XLD (by magnitude) and so the orbital occupancy (towards the $3z^2 - r^2$ orbitals). The spectral features of the unbiased sample resembles those of 14-nm LNO/STO (in gray color) from the substrate-strain experiment except slight differences in the orbital polarization values. (b) Hole occupancy ratio (X, left axis) and orbital polarization (P, right axis) show an irreversible piezoresponse with the V_{bias}.

film and the copper plate underneath the substrate as top and bottom electrodes, respectively, as shown in Fig. 5(a).

The XAS data at the Ni $L_{2,3}$ edges were collected with E_{ab} and E_c x-ray polarizations, similarly to the previous experiment, but using the *in situ* applied V_{bias} (up to ±200 V) to the sample, within the ultrahigh-vacuum chamber of the HECTOR endstation at the BOREAS beamline. In Fig. 5(b), we show the raw TEY signal (before normalizing it to the x-ray absorption (I_{ref}) signal from a Au mesh) for an E_{ab} polarization, collected at 0 V and ±200 V DC. The background current is found to be larger for $V_{\text{bias}} > 0$ than for $V_{\text{bias}} < 0$, because V_{bias} appplied to the sample affects the drain current measured by the electrometer (more details given in Ref. [26]). Naturally, this variation has no significance when calculating the XLD data because we have normalized the XAS data to the averaged L_3-peak intensity (following a protocol identical to that used in the substrate-induced strain experiments). In Figs. 5(c)–5(e) we show the La-subtracted Ni $L_{2,3}$ XAS using V_{bias} = -200, 0, and +200 V, respectively. The integrated intensities were calculated after removing a similar step function from all the XAS.

In Fig. 6(a) we show the XLD data obtained from the spectra in Figs. 5(c)–5(e). We first note that the XLD spectral features for the L_3 and L_2 edges at $V_{\text{bias}} = 0$ V are qualitatively similar, apart from the magnitude, to those observed in the 14-nm LNO film on an STO substrate [see the gray color spectra in Fig. 6(a)]. This confirms that the STO buffer layer induces a tensile strain on the top-lying LNO film of the LNO/STO//PMN-PT heterostructure, just like in the 14-nm LNO/STO film. The determined hole ratio X (≈1.04) and the orbital polarization P(≈ 6%) values for the above unbiased sample are depicted in Fig. 6(b). Interestingly, the observed X and P values are in between those reported above for 14- and 5-nm films on STO [see Figs. 3(b) and 3(a)], and thus they are fully consistent. The XLD in Fig. 6(a) varies when applying the V_{bias} across the PMN-PT, with a virtually identical response to $V_{\text{bias}} > 0$ and $V_{\text{bias}} < 0$. In both cases, the applied voltage induces a more positive XLD signal. Consistently, we note that when increasing $|V_{\text{bias}}|$, irrespective of its polarity, the hole ratio $X = h_{3z^2-r^2}/h_{x^2-y^2}$ decreases, as shown in Fig. 6(b), implying that the $3z^2 - r^2$ electron orbital occupancy increases with the bias.

In Fig. 6(b), the variation of X and P with V_{bias} is shown. Arrows indicate the V_{bias} sequence followed in the experiment (0 V→+200 V→0 V→−200 V→0 V). It is observed that $X(V_{\text{bias}})$ displays a butterfly-like loop. The butterfly-like shape of X,$P(V_{\text{bias}})$ shown in Fig. 6(b) is reminiscent of the piezoresponse of ferroelectric PMN-PT under the electric field. More precisely, the observed hysteretic response is that expected if the PMN-PT follows a minor loop, thus indicating that $V_{\text{bias}} = \pm 200$ V is not large enough to push all the ferroelectric domains of PMN-PT along the [001] direction. This view is confirmed by the direct comparison of the observed XLD(V_{bias}) response with the piezoresponse of a (001) PMN-PT crystal shown and the experimentally observed shifts of the PMN-PT reflections and STO when V-biasing the substrates [26]. Therefore, although no direct evidence of the piezoinduced deformation of the LNO layer is available, the observed expansion of the STO layer under bias and the coherent growth of LNO on STO, strongly supports the view that the LNO layer is also piezodeformed.

Although the minor loops, as mentioned, can be at the origin of the observed hysteresis of XLD(V_{bias}), other scenarios could be envisaged. For instance, Levin *et al.* [37] showed that nonsymmetrical and nonreversible piezodeformation of PMN-PT are observed using x-ray-diffraction experiments sensitive to the (001) PMN-PT crystal surface (probing about 0.5 μm depth), while reversible piezoresponsive butterfly loops were recorded using reflections probing the bulk of the crystal. It was argued that the different response was due to distinctive domain reconstructions at the crystal surface that produce irreversible deformation (i.e., nonelastic) loops. On the other hand, it has also been reported that cracks, quite counterintuitive, can be reversibly formed in PMN-PT upon polarization switching and they can be transferred to the metallic layers grown onto it. In fact, when the coating layer is a metallic alloy (MnPt), substrate cracks can lead to reversible changes of the resistivity of the ductile metallic films [38]. In the same vein, voltage pulses applied to PMN-PT substrates and subsequent morphologic reconstructions have

been shown to promote reversible changes of magnetic and electric properties of ductile metallic Fe_xMn_{1-x} layers [39]. In the present case, the LNO film is not expected to be ductile and so any morphological reconstruction in the substrate should lead to an irreversible response in the LNO film. All in all, this mechanism will give rise to some hysteretic domain configuration and thus a hysteretic strain distribution acting upon the orbital occupancy of the LNO films.

Here, of higher relevance is the discovery that, under V_{bias}, the $3z^2 - r^2$ electron occupancy is clearly favored in a magnitude tunable by the V_{bias}. This observation, together with the butterfly-like response, strongly suggests that the electric-field-induced strain is transmitted from the PMN-PT substrate towards the top-lying LNO film. This observation would be consistent with a clamping of LNO onto the STO-buffered PMN-PT substrate, although it should be recognized that we have not direct (structural) evidence of the piezodeformation of the LNO lattice. Accordingly, a voltage-induced expansion of the substrate along the direction of the applied electric field (perpendicular to the crystal plane) shall produce a contraction in its in-plane lattice parameter and thus the LNO film would be in-plane compressed. The field-induced in-plane compression of the substrate is given by $\Delta a_s/a_s = -d_{31} \times E$, where a_s is the PMN-PT cell-parameter, d_{31} is the transverse piezoelectric coefficient, and E is the applied electric field. As a result, and in agreement with the data collected on LNO films under different epitaxial strain [Fig. 2(c) and Fig. 3(a)], the $3z^2 - r^2$ electron occupancy should be favored, which is fully consistent with the observation. The data in Fig. 6(b) show that the changes in hole and electron orbital occupancies at the largest V_{bias} (± 200 V) are $\Delta X \approx -2.7\%$ ($\Delta X/\Delta\varepsilon = -54\%/\%$) and $\Delta P \approx 3.9\%$ ($\Delta P/\Delta\varepsilon = -78\%/\%$). In order to get a better insight into the significance of these relative changes, we replot in Fig. 3(b) the observed dependence of (X, P) vs V_{bias} (bottom axis) and the voltage-induced strain [$\varepsilon(V_{\text{bias}}) = -d_{31} \times E$] (top axis) developed by the PMN-PT substrate. In this evaluation, we used $d_{31} = -1250$ pm/V, as reported for (001) PMN-PT [40]. Assuming that the LNO is clamped to the STO layer and ultimately to the substrate, and the strain is fully transmitted, this evaluation provides the maximal in-plane compressive strain to be expected from PMN-PT. It is important to note that the maximal voltage-induced strain is of only about -0.05% but the change of polarization is remarkably high (78%/% of $\Delta P/\Delta\varepsilon$), and consequently in Fig. 3(b), the slope of X,$P[\varepsilon(V_{\text{bias}})]$ is exceedingly (about 9 times) larger than the X,$P(\varepsilon)$. We shall comment below on this difference.

IV. SUMMARY AND CONCLUSIONS

We have used XAS and XLD at the Ni $L_{2,3}$ edges to determine the orbital occupancy in $LaNiO_3$ films. Several conclusions emerge from the data reported here. We have observed that the epitaxially induced strain effect alone allows for a substantial tuning of the orbital polarization which, however, remains within a modest $-16\% < P < +8\%$ range. We have also quantified the surface-induced orbital polarization that unavoidably favors the $3z^2 - r^2$ orbital occupation and thus provides a $P_{\text{surface}} \approx -4\%$ that adds or subtracts, depending on the sign of the strain, to the strain-only contribution. Relying on the existing Ni-O hybridization, consistent deductions have been derived from XAS and XLD at the O K edges. Finally, we have observed that the electric-field-induced strain applied on the PMN-PT substrate elastically deforms the STO buffer layer by promoting its in-plane compression and enhances the $3z^2 - r^2$ occupancy in LNO. Therefore, it follows that, although the orbital occupancy can be controlled either *ex situ* by an appropriate epitaxial strain or *in situ* by using piezoelectric substrates, the voltage-controlled strain can only favor the $3z^2 - r^2$ occupancy rather than the $x^2 - y^2$ occupancy required to emulate cuprate HTSc. On the other hand, the intriguing observation that the change of orbital occupancy using a V-biased ferroelectric substrate is much larger than expected on the basis of pure elastic effects at first sight may suggest that electronic reconstructions, including charge transfer may remain, although blurred by the STO spacer. Indeed, it has been reported that at the interface between LNO and ferroelectric $BaTiO_3$ [41] or PZT [42], a subtle charge transfer may occur, that may result in a change of orbital polarization. However, in those cases the observed effects were found to reverse when reversing the sign of the polarization. This is in contrast with our data of Fig. 6(b), where an almost voltage-symmetric effect is observed. This strongly supports the view that the observed voltage-induced large sensitivity of orbital polarization is associated with the compression/expansion of the piezosubstrate. A simple hypothesis that could account for this observation is to recall the rhombohedral nature of LNO and the fact that the NiO_6 octahedra are linked by Ni–O–Ni bonds having a bond angle $\theta \approx 150^\circ$ [4]. As the LNO lattice is coherently grown on STO//PMN-PT, a compression/expansion of the substrate unit cell under voltage biasing could translate into a modification of the Ni–O–Ni bond lengths and angles. Nevertheless, as mentioned, assuming the known bulk values of the piezoelectric coefficient of PMN-PT(001), it appears that voltage-induced strain has a larger effect on orbital polarization than epitaxial strain. It may be argued that, in agreement with early data, the elastic properties of PMN-PT surface differ from those of the bulk. However, it cannot be excluded that epitaxial strain, established during film growth at high temperature, has a different impact on bond topologies than *in operando* piezosubstrates. Finally, we have shown that an electric field applied along the [001] direction on PMN-PT(001) unavoidably favors the $3z^2 - r^2$ orbital occupation. To reverse orbital occupancy towards $x^2 - y^2$, piezoelectric substrates with smaller in-plane parameters that may impose compressive strain on LNO, explore different substrate orientations, or even using pregrown freestanding LNO films anchored to the piezosubstrates, can be viable alternative routes worth to explore.

ACKNOWLEDGMENTS

Financial support from the Spanish Ministry of Science, Innovation and Universities, through the "Severo Ochoa" Program for Centers of Excellence in R&D (Grant No. SEV-2015-0496) and Grant No. MAT2017-85232-R (AEI/FEDER, EU), and from Generalitat de Catalunya (Grant No. 2017 SGR 1377) is acknowledged. We thank Dr. Zhiwei Hu,

Max-Planck-Institute for Chemical Physics of Solids, Germany for helpful discussions. The support and advice from Dr. F. Sánchez on the film growth and Dr. Ignasi Fina for ferroelectric characterization are very much appreciated.

[1] N. Hamada, J. Phys. Chem. Solids **54**, 1157 (1993).
[2] V. I. Anisimov, D. Bukhvalov, and T. M. Rice, Phys. Rev. B **59**, 7901 (1999).
[3] J. Chaloupka and G. Khaliullin, Phys. Rev. Lett. **100**, 016404 (2008).
[4] M. María Luisa, J. Phys.: Condens. Matter **9**, 1679 (1997).
[5] J. Chakhalian, J. M. Rondinelli, J. Liu, B. A. Gray, M. Kareev, E. J. Moon, N. Prasai, J. L. Cohn, M. Varela, I. C. Tung, M. J. Bedzyk, S. G. Altendorf, F. Strigari, B. Dabrowski, L. H. Tjeng, P. J. Ryan, and J. W. Freeland, Phys. Rev. Lett. **107**, 116805 (2011).
[6] M. Wu, E. Benckiser, M. W. Haverkort, A. Frano, Y. Lu, U. Nwankwo, S. Brück, P. Audehm, E. Goering, S. Macke, V. Hinkov, P. Wochner, G. Christiani, S. Heinze, G. Logvenov, H. U. Habermeier, and B. Keimer, Phys. Rev. B **88**, 125124 (2013).
[7] A. S. Disa, D. P. Kumah, A. Malashevich, H. Chen, D. A. Arena, E. D. Specht, S. Ismail-Beigi, F. J. Walker, and C. H. Ahn, Phys. Rev. Lett. **114**, 026801 (2015).
[8] A. S. Disa, F. J. Walker, S. Ismail-Beigi, and C. H. Ahn, APL Mater. **3**, 062303 (2015).
[9] C. Aruta, G. Ghiringhelli, A. Tebano, N. G. Boggio, N. B. Brookes, P. G. Medaglia, and G. Balestrino, Phys. Rev. B **73**, 235121 (2006).
[10] D. Pesquera, G. Herranz, A. Barla, E. Pellegrin, F. Bondino, E. Magnano, F. Sánchez, and J. Fontcuberta, Nat. Commun. **3**, 1189 (2012).
[11] S. J. May, J. W. Kim, J. M. Rondinelli, E. Karapetrova, N. A. Spaldin, A. Bhattacharya, and P. J. Ryan, Phys. Rev. B **82**, 014110 (2010).
[12] M. Salluzzo, J. C. Cezar, N. B. Brookes, V. Bisogni, G. M. De Luca, C. Richter, S. Thiel, J. Mannhart, M. Huijben, A. Brinkman, G. Rijnders, and G. Ghiringhelli, Phys. Rev. Lett. **102**, 166804 (2009).
[13] D. Pesquera, M. Scigaj, P. Gargiani, A. Barla, J. Herrero-Martín, E. Pellegrin, S. M. Valvidares, J. Gázquez, M. Varela, N. Dix, J. Fontcuberta, F. Sánchez, and G. Herranz, Phys. Rev. Lett. **113**, 156802 (2014).
[14] Y. Yang, M. Meng Yang, Z. L. Luo, H. Huang, H. Wang, J. Bao, C. Hu, G. Pan, Y. Yao, Y. Liu, X. G. Li, S. Zhang, Y. G. Zhao, and C. Gao, Appl. Phys. Lett. **100**, 043506 (2012).
[15] G. Radaelli, D. Petti, E. Plekhanov, I. Fina, P. Torelli, B. R. Salles, M. Cantoni, C. Rinaldi, D. Gutiérrez, G. Panaccione, M. Varela, S. Picozzi, J. Fontcuberta, and R. Bertacco, Nat. Commun. **5**, 3404 (2014).
[16] A. Tkach, A. Kehlberger, F. Büttner, G. Jakob, S. Eisebitt, and M. Kläui, Appl. Phys. Lett. **106**, 062404 (2015).
[17] C. Thiele, K. Dörr, O. Bilani, J. Rödel, and L. Schultz, Phys. Rev. B **75**, 054408 (2007).
[18] N. B. Aetukuri, A. X. Gray, M. Drouard, M. Cossale, L. Gao, A. H. Reid, R. Kukreja, H. Ohldag, C. A. Jenkins, E. Arenholz, K. P. Roche, H. A. Dürr, M. G. Samant, and S. S. P. Parkin, Nat. Phys. **9**, 661 (2013).
[19] S. Heo, C. Oh, M. J. Eom, J. S. Kim, J. Ryu, J. Son, and H. M. Jang, Sci. Rep. **6**, 22228 (2016).
[20] H. Chen, Q. Qiao, M. S. J. Marshall, A. B. Georgescu, A. Gulec, P. J. Phillips, R. F. Klie, F. J. Walker, C. H. Ahn, and S. Ismail-Beigi, Nano Lett. **14**, 4965 (2014).
[21] D. Preziosi, M. Alexe, D. Hesse, and M. Salluzzo, Phys. Rev. Lett. **115**, 157401 (2015).
[22] J. Heidler, C. Piamonteze, R. V. Chopdekar, M. A. Uribe-Laverde, A. Alberca, M. Buzzi, A. Uldry, B. Delley, C. Bernhard, and F. Nolting, Phys. Rev. B **91**, 024406 (2015).
[23] J. Heidler, M. Fechner, R. V. Chopdekar, C. Piamonteze, J. Dreiser, C. A. Jenkins, E. Arenholz, S. Rusponi, H. Brune, N. A. Spaldin, and F. Nolting, Phys. Rev. B **94**, 014401 (2016).
[24] M. C. Weber, M. Guennou, N. Dix, D. Pesquera, F. Sánchez, G. Herranz, J. Fontcuberta, L. López-Conesa, S. Estradé, F. Peiró, J. Iñiguez, and J. Kreisel, Phys. Rev. B **94**, 014118 (2016).
[25] D. Pesquera, X. Marti, V. Holy, R. Bachelet, G. Herranz, and J. Fontcuberta, Appl. Phys. Lett. **99**, 221901 (2011).
[26] See Supplemental Material at http://link.aps.org/supplemental/10.1103/PhysRevMaterials.4.044404 for (1) structural and electric characterization (S1), (2) temperature dependence of XAS/XLD (S2), (3) XAS analysis: substrate-induced strain (S3), (4) XLD analysis: substrate-induced strain (S4), (5) XLD of capped LNO films (S5), (6) oxygen XAS/XLD (S6), (7) TEY signal (S7), and (8) XLD/XRD data (S8) for electric-field biased experiments. Also see Refs. [43–46].
[27] E. Benckiser, M. W. Haverkort, S. Brück, E. Goering, S. Macke, A. Frañó, X. Yang, O. K. Andersen, G. Cristiani, H.-U. Habermeier, A. V. Boris, I. Zegkinoglou, P. Wochner, H.-J. Kim, V. Hinkov, and B. Keimer, Nat. Mater. **10**, 189 (2011).
[28] W. B. Wu, D. J. Huang, G. Y. Guo, H. J. Lin, T. Y. Hou, C. F. Chang, C. T. Chen, A. Fujimori, T. Kimura, H. B. Huang, A. Tanaka, and T. Jo, J. Electron Spectrosc. Relat. Phenom. **137–140**, 641 (2004).
[29] M. Zangrando, M. Finazzi, G. Paolucci, G. Comelli, B. Diviacco, R. P. Walker, D. Cocco, and F. Parmigiani, Rev. Sci. Instrum. **72**, 1313 (2001).
[30] A. Barla, J. Nicolas, D. Cocco, S. M. Valvidares, J. Herrero-Martin, P. Gargiani, J. Moldes, C. Ruget, E. Pellegrin, and S. Ferrer, J. Synchrotron Radiat. **23**, 1507 (2016).
[31] J. S. Kang, S. S. Lee, G. Kim, H. J. Lee, H. K. Song, Y. J. Shin, S. W. Han, C. Hwang, M. C. Jung, H. J. Shin, B. H. Kim, S. K. Kwon, and B. I. Min, Phys. Rev. B **76**, 195122 (2007).
[32] D. Meyers, S. Middey, M. Kareev, M. van Veenendaal, E. J. Moon, B. A. Gray, J. Liu, J. W. Freeland, and J. Chakhalian, Phys. Rev. B **88**, 075116 (2013).
[33] C. Piamonteze, F. M. F. de Groot, H. C. N. Tolentino, A. Y. Ramos, N. E. Massa, J. A. Alonso, and M. J. Martínez-Lope, Phys. Rev. B **71**, 020406(R) (2005).
[34] F. Y. Bruno, K. Z. Rushchanskii, S. Valencia, Y. Dumont, C. Carrétéro, E. Jacquet, R. Abrudan, S. Blügel, M. Ležaić, M. Bibes, and A. Barthélémy, Phys. Rev. B **88**, 195108 (2013).

[35] O. E. Peil, M. Ferrero, and A. Georges, Phys. Rev. B **90**, 045128 (2014).

[36] J. Varignon, M. N. Grisolia, J. Íñiguez, A. Barthélémy, and M. Bibes, npj Quantum Mater. **2**, 21 (2017).

[37] A. A. Levin, A. I. Pommrich, T. Weißbach, D. C. Meyer, and O. Bilani-Zeneli, J. Appl. Phys. **103**, 054102 (2008).

[38] Z. Q. Liu, J. H. Liu, M. D. Biegalski, J. M. Hu, S. L. Shang, Y. Ji, J. M. Wang, S. L. Hsu, A. T. Wong, M. J. Cordill, B. Gludovatz, C. Marker, H. Yan, Z. X. Feng, L. You, M. W. Lin, T. Z. Ward, Z. K. Liu, C. B. Jiang, L. Q. Chen, R. O. Ritchie, H. M. Christen, and R. Ramesh, Nat. Commun. **9**, 41 (2018).

[39] G. Vinai, F. Motti, V. Bonanni, A. Y. Petrov, S. Benedetti, C. Rinaldi, M. Stella, D. Cassese, S. Prato, M. Cantoni, G. Rossi, G. Panaccione, and P. Torelli, Adv. Electron. Mater. **5**, 1900150 (2019).

[40] R. Zhang, B. Jiang, and W. Cao, J. Appl. Phys. **90**, 3471 (2001).

[41] J. J. Peng, C. Song, B. Cui, F. Li, H. J. Mao, G. Y. Wang, and F. Pan, Appl. Phys. Lett. **107**, 182904 (2015).

[42] M. S. J. Marshall, A. Malashevich, A. S. Disa, M.-G. Han, H. Chen, Y. Zhu, S. Ismail-Beigi, F. J. Walker, and C. H. Ahn, Phys. Rev. Appl. **2**, 051001 (2014).

[43] M. Medarde, A. Fontaine, J. L. García-Muñoz, J. Rodríguez-Carvajal, M. de Santis, M. Sacchi, G. Rossi, and P. Lacorre, Phys. Rev. B **46**, 14975 (1992).

[44] J. W. Freeland, M. van Veenendaal, and J. Chakhalian, J. Electron Spectrosc. Relat. Phenom. **208**, 56 (2016).

[45] P. Kuiper, G. Kruizinga, J. Ghijsen, G. A. Sawatzky, and H. Verweij, Phys. Rev. Lett. **62**, 221 (1989).

[46] T. Jiang, S. Yang, Y. Liu, Y. Yin, S. Dong, W. Zhao, and X. Li, Appl. Phys. Lett. **103**, 053504 (2013).